The role of morphology in setting the fate of marine snow in the open ocean

Stemmann Lars[1,2,*], Ariadna C. Nocera[1], Marin Arlaud[1], Joelle Habib[1], Alberto Baudena[3], Alexandre Accardo[1], Jean Olivier Irisson[1], Léo Lacour[1], Philip W. Boyd[4], Rainer Kiko[5],

[1]Sorbonne Université, CNRS, UMR 7093, Institut de la Mer de Villefranche sur mer, Laboratoire d'Océanographie de Villefranche, Villefranche‑sur‑Mer, France
[2]Institut Universitaire de France, France
[3]National Research Council - Institute of Marine Sciences (CNR-ISMAR), Lerici (SP), Italy
[4]Institute for Marine and Antarctic Studies, University of Tasmania, Hobart, Australia
[5] GEOMAR Helmholtz Centre for Ocean Research Kiel, Kiel, Germany

- corresponding author: lars.stemmann@sorbonne-universite.fr

Supplementary material

SM1: The BGC-Argo floats deployment

The data were produced by four BGC-Argo (BioGeochemical-Argo) floats: WMO: 59006623, 6903095, 6903096,6904139) deployed respectively in the regions of southern Tasmania, Benguela, Angola and Ecuador (Figure 1). These floats were equipped with a Sea-Bird SBE 41 CTD, a Sea-Bird ECO triplet probe to measure fluorescence at 470 nm and backscatter volume at 700 nm with an angle of 124°, an Aanderaa oxygen optode probe and an Underwater Vision profiler 6 Low-power (UVP6-LP) in-situ camera (Picheral et al. 2022). Only data acquired during ascent are analysed. The floats completed a total of 680 profiles, with 86 profiles in Ecuador between 14/07/2021 and 23/03/2022, 118 in Angola between 05/05/2021 and 26/04/2022, 184 in Benguela between 13/04/2021 and 17/09/2022, and 294 in Tasmania between 13/12/2020 and 16/11/2023. The frequency of ascending profiles in Ecuador is on average 2 days 23 hours ± 1 day 9 hours, in Angola 3 days 1 hour ± 20 hours, in Benguela 2 days 20 hours ± 15 hours, and in Tasmania 3 days 15 hours ± 3 days 12 hours. Tasmania stands out with a sampling frequency that varies over time, with a maximum of two profiles 12 hours apart during spring and summer and 1 profile every 10 days during the Australian winter.

Float data are collected from the post-processed dataset, improving the processing of chlorophyll a (Schmechtig et al., 2025). The derived physical variables Absolute Salinity (AS), Conservative Temperature (CT, °C), Potential Density (kg m^{-3}) with a reference depth of 0 (Roquet et al., 2015) and Solubility (S, kg m^{-3}) with a reference depth of 100 m (Roquet et al., 2015) are used to calculate the oceanographic Conservative Temperature (CT, °C), Potential Density (kg m^{-3}) with a reference depth of 0 m (Roquet et al., 2015) and oxygen solubility (µmol kg^{-1}) were calculated using the Python implementation of the Gibbs SeaWater Oceanographic Toolbox based on the Thermodynamic Equation of Seawater – 2010. Apparent oxygen utilisation based on Thermodynamic Equation of Seawater – 2010. Apparent oxygen use (AOU, µmol kg^{-1}) was calculated as the difference between oxygen solubility and the measured concentration of dissolved oxygen (DOXY, µmol kg^{-1}). The MLD was calculated in two manners (Lacour 2019). The MLDbio is kept for the rest

of the manuscript because it corresponded more with the Chla, BBS and marine snow vertical gradient. The volume of backscattering particles at 700 nm is converted into a particle backscattering coefficient (Bbp700, m^{-1}) following standard BGC-Argo procedures. The Bbp signal is broken down into three components described in Briggs et al. (2020): Bbs, Bbl and Bbr. Bbl is the backscattering component due to the largest particles (> 100µm), Bbs is the component due to the smallest particles (< 100µm) and Bbr is the deep bed (Briggs et al. 2020). The particles detected by the UVP are automatically classified into two size groups: micrometric particles (MIP) with a size range between 0.1 and 0.5 mm in Equivalent Spherical Diameter (ESD) and macrometric particles (MAP) with a size range between 0.5 and 16 mm. Only Bbs, MIP and MAP will be used, as Bbl overlaps the size ranges. Marine snow solid aerial (MSSa) concentration is calculated as the sum of the grey values of the pixels in each object times their area.

We restricted the time period explored in the manuscript for the statistical analysis to the largest common time window shared between the four deployments, between the latest sampling start date and the earliest sampling end date. This time window corresponded to the shortest period at the Equator, starting on 14/07/2021 and ending on 23/03/2022. However, to visualize patterns on a more extended period in Angola, Benguela and Tasmania, the time series figures start on **01/04/2021 and end on 01/05/2022. T**o reduce the weight of intra-daily variability in high-frequency day-night profiles only present in Tasmania, we selected night profiles in this region. A total of 293 profiles were retained, with 83 profiles in Ecuador, 74 profiles in Angola, 84 profiles in Benguela and 52 profiles in Tasmania. To reduce the number of data which come in quasi-continuous depth profiles and to increase the number of marine snow and plankton counts in the statistical analysis we assembled the data in three depth layers of varying depths. The first one from surface to MLD_bio with a range of observed volume (mean = 0.4 m^3, range 0.05 - 1.68 m^3) per profiles, the second one from the lower limit of the previous layer adding 400 m depth (MLD_bio+400) with a range of observed volume (mean = 1.04 m^3, range 0.32 - 2.19 m^3) per profiles, and the third one from MLD_bio+400 to 1000 m depth with a range of observed volume (mean = 0.6 m^3, range 0.03 - 0.95 m^3) per profiles. Finally, statistical analysis is presented in this work only for the upper and deepest layers to enhance the contrasts.

Several Lagrangian diagnostics were performed using satellite data. For each station, a circle with a diameter of 0.1° was defined and filled with particles separated by 0.01°. Each particle is then advected backwards in time, following a current velocity field derived from altimetry and a deferred model including geostrophic and Ekman components. The advective time varies from 5 to 45 days. Two metrics were used: Finite-time Lyapunov Exponents (FTLE, days−1; Shadden et al. 2005), which is a measure of the intensity of frontal structures, and the Lagrangian chlorophyll a (LC in mg m−3), which is the average chlorophyll a content calculated along the particle's trajectory. The selection of advective time is performed individually for each variable. Spearman correlations between the target variable and marine snow morphology concentrations were calculated. For each advective time, the absolute values of the significant correlations were summed. The optimal advective time for each variable was then defined as the time period yielding the highest total sum of absolute significant correlations.

SM2: Image classification for zooplankton and Marine Snow

Images of objects larger than 670 µm were saved in the UVP6's internal memory and downloaded when recovered. The images were processed after download by UVP App 2 V2.2 and V2.3 and imported into the EcoTaxa web application for individual classification (https://ecotaxa.obs-vlfr.fr/). As the identifications were carried out by different teams, the dataset was checked to ensure the consistency of identifications between observers. The verification was carried

out on a sub-sample, the number of which was determined by identification category using Monte Carlo simulations in order to detect an error rate of 5% with a confidence interval of 95%. The taxa included in the analysis (Table XX) were selected based on their abundance across the study regions, their ecological relevance to the study, and practices in the literature (Drago et al. 2022; Panaïotis et al. 2023). Copepoda and associated groups were separated into big and small copepods with an ESD greater than 1 mm and less or equal to 1 mm, respectively.

Marine Snow classification was carried out by constructing a morphological space based on their morphological characteristics. This space is then used to project each of the objects into it, allowing us to group objects with morphological similarities into groups called morphs. The morphological space was constructed following Trudnowska et al. (2021) by a weighted principal component analysis (wPCA) on the 666,126 processed images of detritus. The number of components retained was determined using the Kaiser-Guttman criterion (Cattell 1966). The selection of morphological features to be included in the analysis (Table XX) was based on a parsimonious approach between the choices made in previous studies (fractal dimension was excluded because UVP6 images from the float in Tasmania were processed differently than those from the other three floats) and the model including all features and a selection by algorithm called the Escouffier method. The algorithm works by selecting and adding, by permutation, the morphological characteristics that maximise the vector rho coefficient (RV) (Robert et al. 1976) between the coordinates of objects in a principal component analysis (PCA) performed on the total model and in a PCA performed on the selected characteristics. The ability of the different models to create a discriminating morphological space is compared by following the proportion of variance explained on the first axis of the wPCA. The selected morphological characteristics were thresholded to remove the 0.1% of lower and upper outliers. Individuals with more than 5 missing values were considered too extreme and removed from the analysis (n = 484). The other missing values were replaced by the mean values of the corresponding characteristic, as this manipulation did not influence the wPCA. A Yeo-Jonhson transformation (Yeo et al. 2000) was then applied to all characteristics.

The resulting global dataset comprises 1,059,238 images, of which 106,440 were classified as plankton and 889,345 as detritus (the rest being artefacts or bad focus objects). Supplementary Table XX: Morphology properties of marine snow images used to calculate the morphospace.

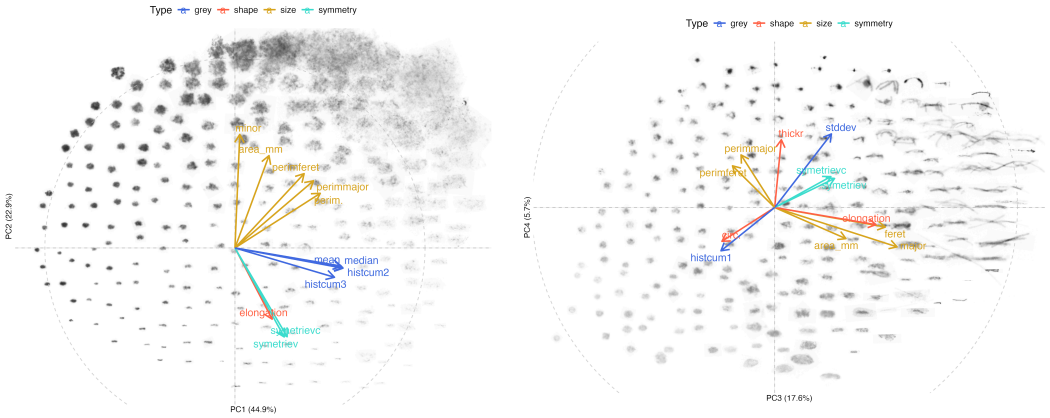

Supp. Figure 1 : Marine Snow morphospace along PC1/PC2 and PC3 and PC4

To create the clusters, we performed a k-means weighted by observations (Hartigan et al. 1979) with a fixed number of clusters set at 200 on the coordinates of the objects along the axes of the selected morphological space. We then determined the coordinates of the centroids of each group,

calculated the Euclidean distance matrix of these, and applied agglomerative hierarchical clustering using Ward's method (Supp. Fig. 2a). The optimal number of clusters to be created was determined following previous studies[1–4] and following an approach using the Shannon-Wiener diversity index. For this latter approach, the Shannon-Wiener index was calculated for each level of the hierarchical tree between 1 and 200 groups. This allows us to understand the evolution of entropy for each choice of number of groups. As expected, the higher the number of groups formed, the higher the associated entropy. We therefore focused on the second derivative of entropy (Supp. Fig. 2b) to detect the two first minima (for 5 and 17 clusters) in the change of the entropy.

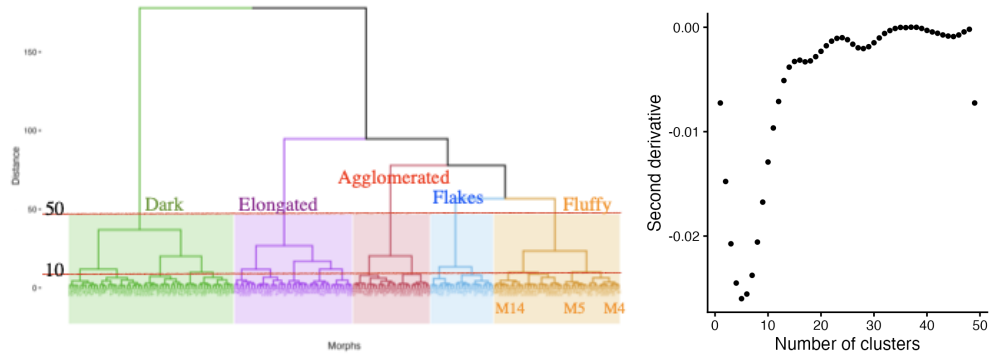

Supp. Figure 2: a) Hierarchical Clustering showing the two layers or image grouping at 5 and 17 levels, b) second derivative of the change in entropy as number of groups increases.

SM 3: Description of Marine Snow Morphotypes

To improve upon previous marine snow classification methodology[1], we added a hierarchical clustering approach, reducing the number of morphotypes from 200 to 5 parents and 17 children categories. This method not only simplifies the interpretation but also maintains ecological relevance. It also strengthens the statistical power of the associations made by having higher abundances per group (in the five categories relative to the 17), and respects a more parsimonious approach for classifying detritus according to morphology[1] when the number of explanatory variables is low. We retain the established nomenclature: flakes, dark, fluffy, elongated, and agglomerates[1] for the parent groups, while at level 17, they will be referred to as MX (*X* varying from 1 to 17). Table 1 summarizes the key properties of the five parent morphotypes, including their mean grey level, circularity, and area. This classification was compared to the original ones in the three previous studies[2–4] and showed very consistent patterns with previous results[2,4,5] in distinguishing morphotypes of particles being classified in similar types (SM 3). This refined classification based on the four datasets allows for comparable ecological insights into the impact of marine snow morphology on its vertical export. It is noticeable that our modified method yields five main types of morphological groups as in the previous works with the advantage that they can be subdivided hierarchically. Interestingly, existing classifications based on the observation of collected or produced detritus also divide the immense diversity of morphologies into a similar number of groups[6–9].

Parent-morphotypes	Parent-morphotypes images	Child-morphotypes sketched at scale
Flakes 79 325 images - Mean grey level = 202, IQR = 12.3 - Circularity = 0.205, IQR = 0.11 - Area = 0.69 mm², IQR = 0.56	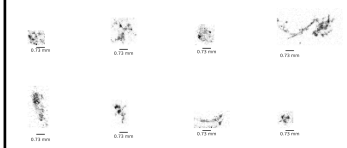	
Dark 192 337 images - Mean grey level = 150, IQR = 17.7 - Circularity = 0.74, IQR, = 0.26 - area = 0.58 mm², IQR = 0.37	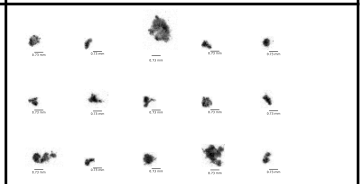	
Fluffy 185 328 images - Mean grey level = 185, IQR = 23.5 - Circularity = 0.506, IQR = 0.25 - Area = 0.52 mm², IQR = 0.22	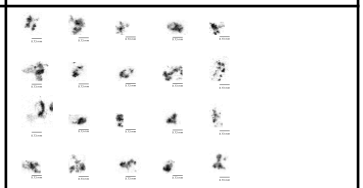	
Elongated 133 012 images - Mean grey level = 172, IQR = 23.5 - Circularity = 0.31, IQR, 0.23 - Area = 0.54 mm², IQR = 0.27	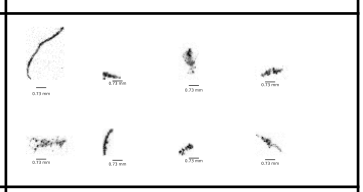	
Agglomerates 76 212 images - Mean grey level = 177, IQR = 21.6 - Circularity = 0.3 , IQR = 0.2 - Area = 2.03 mm², IQR = 1.87	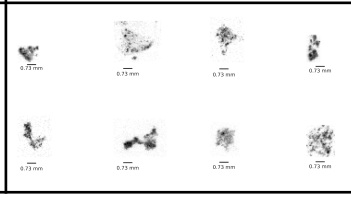	

Table 1: Parent marine snow morphotypes properties grouped at 5 levels and examples of images sorted in the 17 child-morphotypes. IQR: interquartile range. A subset of 8 up to 20 images randomly sampled from each morph is given. Drawings were made from the mask of selected marine snow

particles, respecting size (scale bar is 1 mm), shape, and opacity to better visualize the 17 child-morphotypes.

In the vignettes, light colors (high grey levels) correspond to transparent matter and dark colors correspond to matter that strongly reflects light such as dense organic or mineral material. The **flakes** category consists of the lightest objects (median average grey level = 202, IQR = 12.3), which are not very circular (median circularity = 0.205± 0.11) and are relatively larger (median size = 0.69 mm², IQR = 0.56). ± 0.11) (Supp Fig 5). The 2 flake child categories (M1 and M2), are surface particles differing mainly by their size (M2 with an area of 1mm^2 being larger than M1). **Dark** category contains the darkest objects (median grey level = 150, IQR = 17.7), of intermediate size (median area = 0.58 mm², IQR = 0.37) and circular (median circularity = 0.74 IQR = 0.26) mostly found below the MLD (apart for M6). **Dark** category, further divided into 5 categories (M3, M6, M8, M15, M16) that differ mainly by their size (M3 >1mm^2) and circularity with M15 being most circular and M16 the least. The **fluffy** category consists of objects more circular (median circularity = 0.506, IQR = 0.25), and relatively small (median area = 0.52 mm², IQR = 0.22) mostly found above or associated with the MLD. Fluffy particles, further divided in 3 categories (M4, M5, M14) that differ mainly by their circularity with M4 being more circular than M5 and M14. The **elongated** category contains the most elongated objects (median elongation = 3.27, IQR = 2.41) of intermediate size (median area = 0.54 mm², IQR = 0.27) and grey (median average grey level = 172, IQR = 23.5). They are sub-divided in 5 categories according to their morphological properties and depth distribution. M12 and M17 are almost exclusively found above the MLD and they are the most elongated but differ by their grey level, morphotype 12 being more bright and complex (kurtosis high). M7, M9 and M10 can be found below the MLD (specially M10) and they are less elongated. They differ by their mean grey level with darker particles in the following order M7, M9, M10. The category **agglomerated** consists of large objects (median area = 2.03 mm², IQR = 1.87), light (median average grey level = 177, IQR = 21.6) and not very circular (median circularity = 0.30 , IQR = 0.20). It contains two sub-categories which have the same size distribution but differ mainly by the grey level and their vertical positioning, M13 being much darker and deeper than M11.

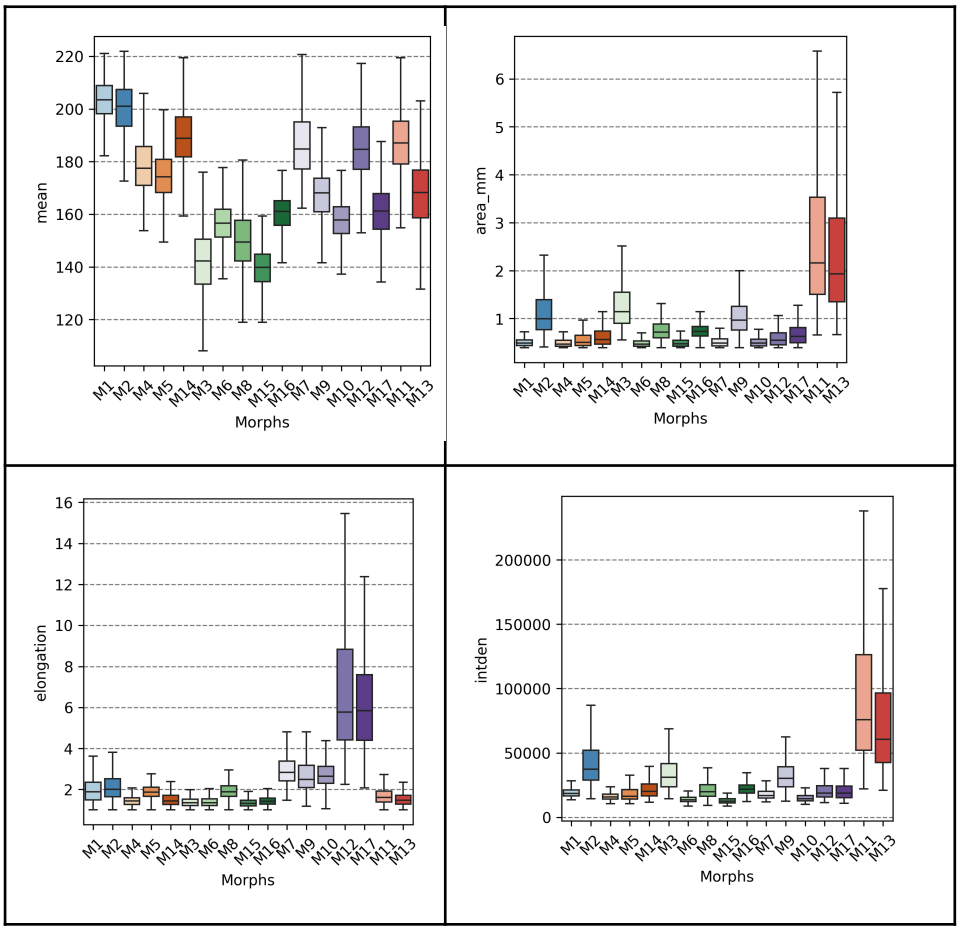

Supp Figure 3: Morphological properties of the 17 morphotypes: a) grey level (from 1 (black object) to 256 (white object), b) area in mm^2, c) elongation (dimensionless), e) integrated density. Integrated density, corresponds to the sum of the grey values of the pixels within the object.

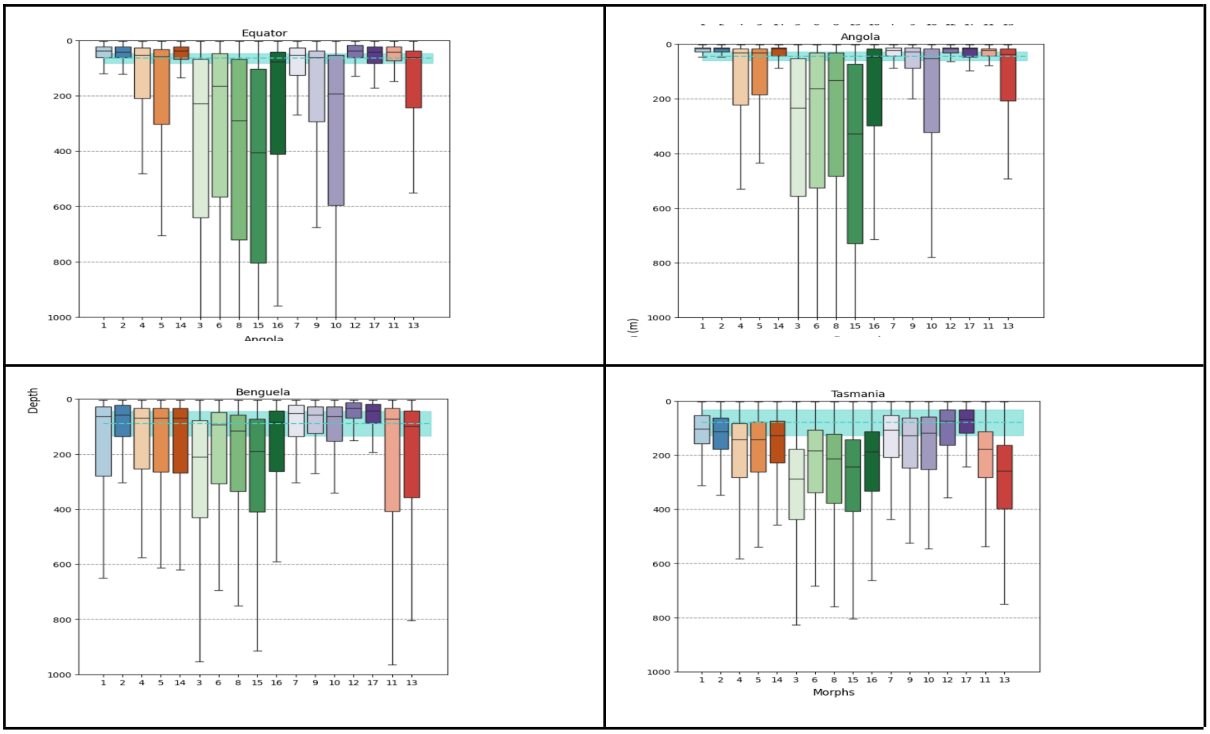

Supplementary Figure 4: Vertical distribution of the 17 morpho-clusters in A) Equator, B) Angola, C) Benguela, D) Tasmania. The seasonal depth range of the MLD-bio is reported in each region.

SM 4: Comparison with the previous marine snow classification

Morphotypes	Habib et al., 2025	Soviadan et al., 2025	Accardo et al., 2025
Flakes	Small Porous particles 7% **Big Porous particles 82%** Fiber particles 10% Small dense particles 0% Big dense particles 0%	**Flakes 79%** Spheres 0% Strings 9% Agglomerate 12%	**Bright 100% (96%)** Small 0% Elongated 0% (4%) Aggregated 0%
Dark	Small Porous particles 7% Big Porous particles 0% Fiber particles 0% **Small dense particles 61%** **Big dense particles 32%**	Flakes 0% **Spheres 83%** Strings 0% Agglomerate 17%	Bright 1% (1%) **Small 67% (66%)** Elongated 0% **Aggregated 32% (32%)**
Fluffy	**Small Porous particles 68%** Big Porous particles 15% Fiber particles 7% Small dense particles 8% Big dense particles 2%	**Flakes 36%** **Spheres 47%** Strings 7% Agglomerate 10%	**Bright 59% (71%)** **Small 33% (23%)** Elongated 3% (3%) Aggregated 5% (3%)
Elongated	Small Porous particles 9% Big Porous particles 6% **Fiber particles 68%** Small dense particles 7% Big dense particles 10%	Flakes 12% Spheres 9% **Strings 71%** Agglomerate 9%	Bright 5% (11%) **Small 21% (9%)** **Elongated 62% (74%)** Aggregated 11% (6%)
Agglomerates	Small Porous particles 0% **Big Porous particles 35%** Fiber particles 0% Small dense particles 0% **Big dense particles 65%**	Flakes 2% Spheres 0% Strings 0% **Agglomerate 98%**	Bright 6% (37%) Small 0% Elongated 0% (2%) **Aggregated 94% (61%)**

Table XX: Percentage of the different morphs in this study that match the morph classification in previous publication.

SM 5: Marine Snow and Plankton community structure during the annual survey

	Flakes		Dark					Fluffy			Elongated					Agglomerated	
	M1	M2	M3	M6	M8	M15	M16	M4	M5	M14	M7	M9	M10	M12	M17	M11	M13
Equator	6.0% 2.1% *0.6%*	6.6% 2.4% *0.7%*	3.6% **10.5%** **10.9%**	8.2% **14.1%** **18.1%**	3.8% 9.8% **14.3%**	2.5% **10.1%** **16.7%**	2.9% 3.6% 3.4%	6.7% 5.2% 4.3%	8.4% 7.9% 6.9%	**19.4%** 8.3% 4.8%	6.9% 4.6% 3.3%	2.9% 3.0% 2.2%	3.1% 5.6% 7.0%	4.5% 1.5% *0.8%*	3.7% 2.0% *1.1%*	5.0% 2.6% *1.1%*	5.8% 6.7% 3.8%
Angola	8.1% 3.0% *0.9%*	**11.8%** 4.5% *1.3%*	*1.8%* 7.9% **12.2%**	4.4% **11.6%** **19.8%**	2.1% 6.2% 9.4%	*1.0%* 4.6% **10.1%**	*1.4%* 2.3% 2.6%	6.9% 8.8% 9.0%	7.5% 9.0% 8.0%	**20.5%** **12.9%** 7.1%	8.3% 4.9% 3.2%	2.3% 2.3% *1.6%*	*1.6%* 2.5% 3.3%	6.1% 2.7% *1.1%*	3.2% *2.0%* *1.2%*	6.8% 4.9% *1.8%*	6.4% **10.0%** 7.4%
Benguela	3.9% 2.3% 3.0%	4.1% 1.8% 2.8%	3.1% 8.5% **10.2%**	8.6% **11.7%** **11.5%**	5.3% **11.0%** 8.6%	6.1% **15.6%** **17.3%**	2.4% 3.1% 2.6%	4.8% 3.1% 4.8%	6.2% 4.9% 6.5%	**12.1%** 7.5% **11.8%**	6.9% 3.5% 4.3%	4.3% 4.0% *2.0%*	8.1% 7.7% 4.5%	6.8% 2.2% *1.8%*	**12.7%** 8.7% 2.2%	*2.0%* *1.3%* 2.7%	2.5% 3.2% 3.5%
Tasmania	7.9% 5.2% 2.4%	9.3% 6.7% 3.8%	*2.0%* 6.1% **11.4%**	6.2% 9.5% **10.6%**	3.4% 6.4% 8.9%	2.9% 6.6% **10.9%**	*1.9%* 3.0% 3.0%	4.4% 4.6% 4.2%	7.4% 7.6% 6.2%	**16.0%** **14.4%** 9.1%	7.8% 4.8% 4.0%	4.1% 3.3% 2.7%	5.4% 3.8% 3.9%	6.1% *1.9%* 1.8%	8.1% 2.1% *1.4%*	4.2% 6.9% 5.3%	2.7% 7.1% **10.5%**

Table 1: Contribution of different morphs to total marine snow at each site and in three layers: epipelagic (0-MLD), upper (MLD-MLD+400m), and lower mesopelagic (MLD+400-1000m). Contributions of more than 10% are set in bold. Those less than or equal to 2% are in italic.

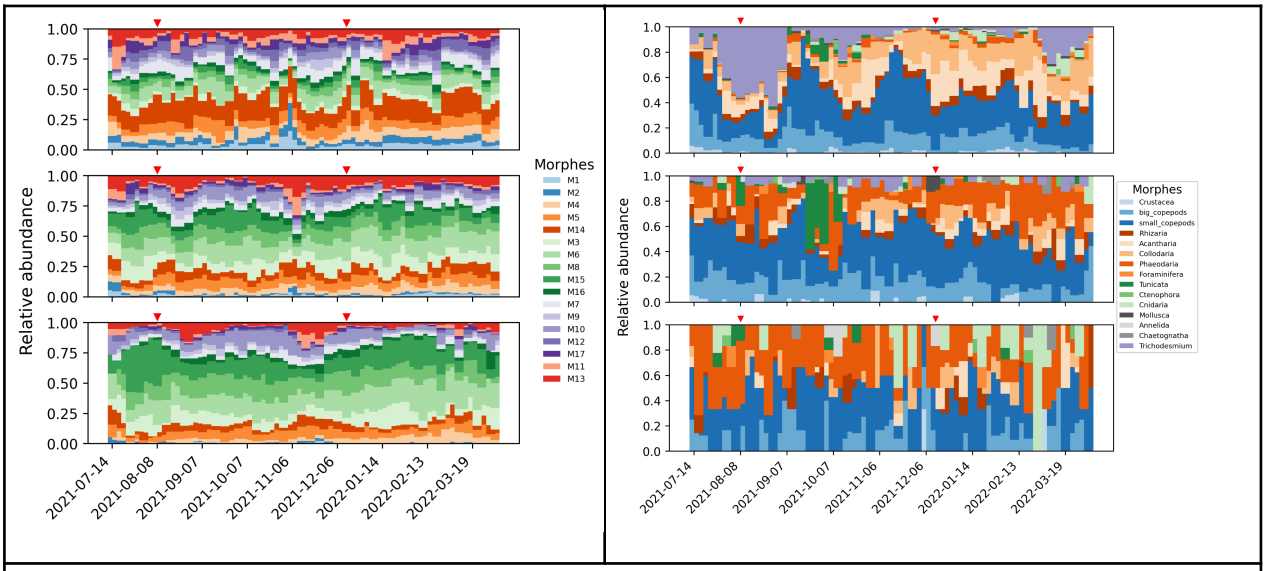

Supplementary Figure 5A: Annual variability of marine snow (left column) and zooplankton (right column) community compositions during the deployment at the Equator. Red triangles indicate the events.

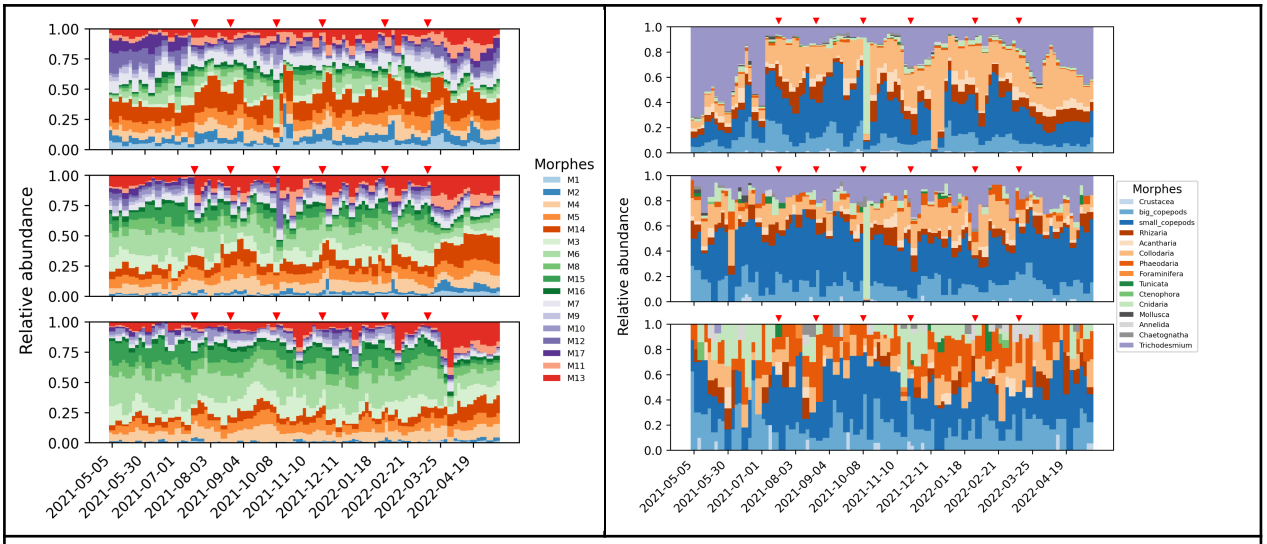

Supplementary Figure 5B: Annual variability of marine snow (left column) and zooplankton (right column) community compositions during the deployment off Angola. Red triangles indicate the events.

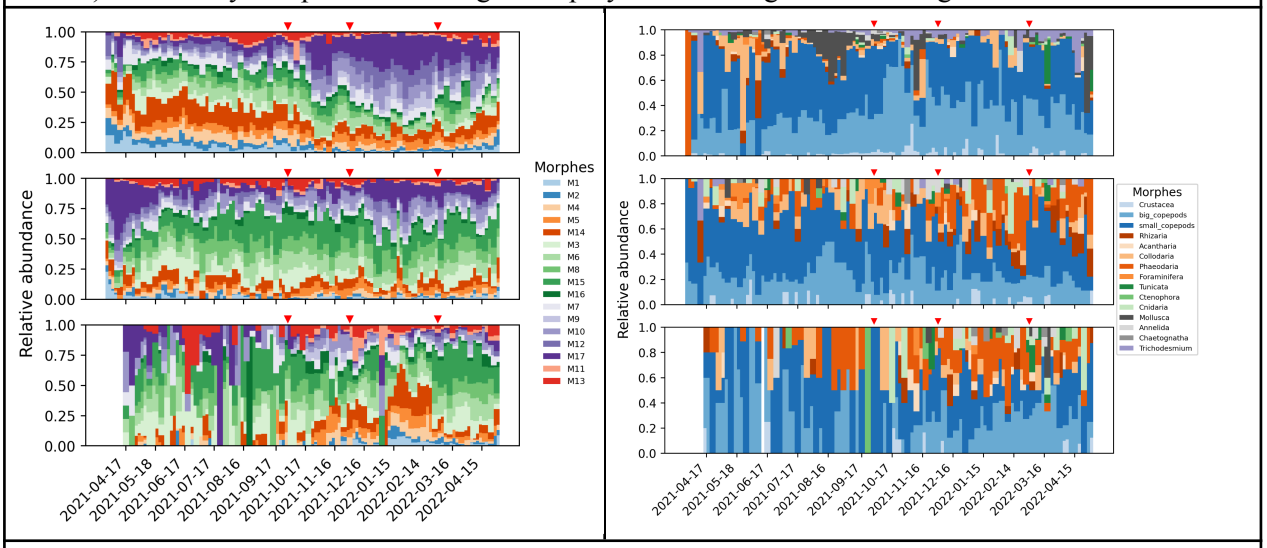

Supplementary Figure 5C: Annual variability of marine snow (left column) and zooplankton (right column) community compositions during the deployment off Benguela. Red triangles indicate the events.

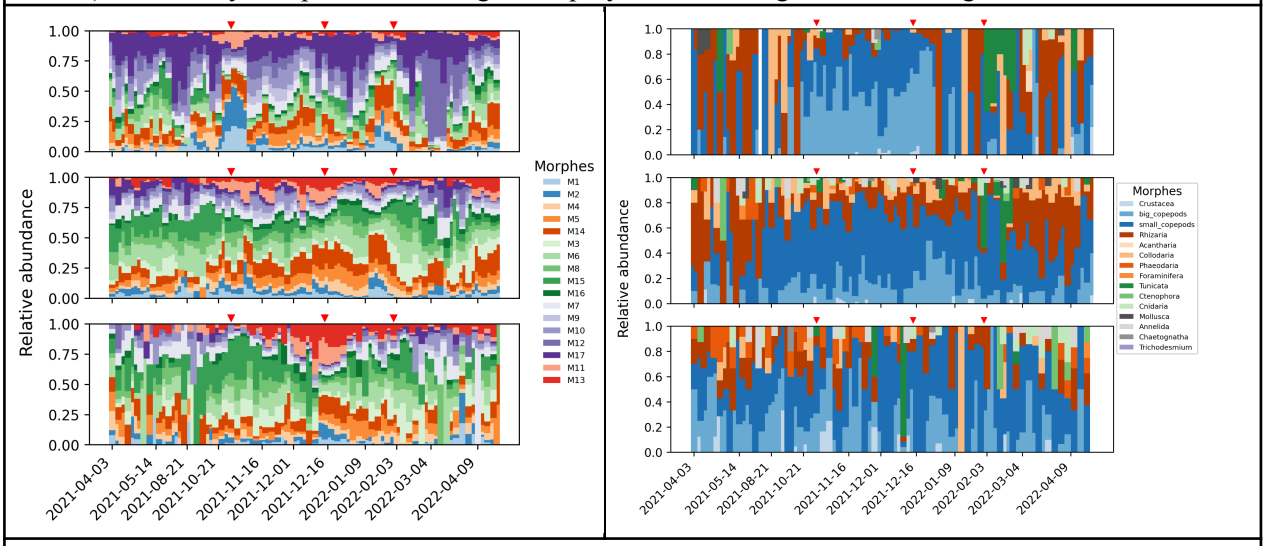

Supplementary Figure 5D: Annual variability of marine snow (left column) and zooplankton (right column) community compositions during the deployment off Tasmania. Red triangles indicate the events.

SM 6: Correlations between Marine snow and environment

Here, we will try to further assess the ecological relevance of 17 MS morphotypes by analysing their temporal dynamics and their correlation with concomitant plankton assemblages and environmental data (in situ Temperature, Salinity, O2, Chla, bbs).

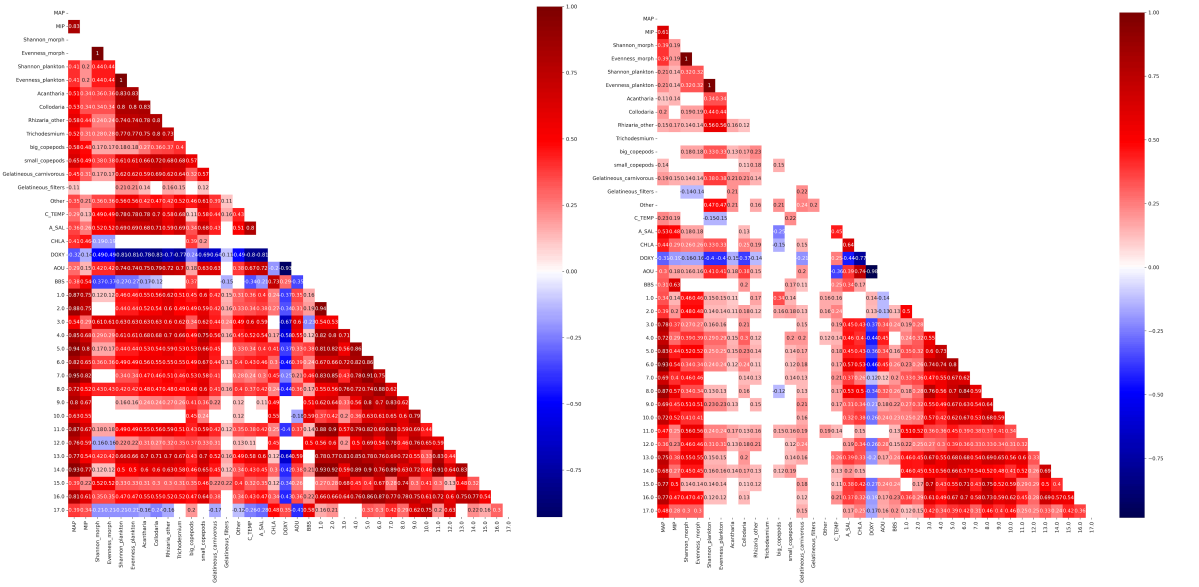

Supp. Figure 6:. Spearman Correlation with abiotic and biotic variables in mixed layer (left) and in lower mesopelagic (right)

Flakes (M1 and M2) overall contribution to the total community is low (<10%) in both layers of the four regions apart from few specific events (up to 40% in the mesopelagic layer of Tasmania, Supp. Fig XX). Their temporal dynamics as shown by the PCA, is similar (Figure 7). Their correlation with in situ Chla is low (rs<0.2) but increases considering the LLC (rs>0.4 for lag >) suggesting that their accumulation requires the aggregation to take place over a long lasting phytoplanktonic production (XX days). They also have a strong correlation with Rhizarians, Trichodesmium and small copepods (rs>0.5) suggesting that they are formed by diverse phyto- and zoo-planktonic processes in the trophic web. Their mostly round shape suggests the coagulation as a mechanism to aggregate the different source particles. What looked like voids in images might have been transparent exopolymer particles (TEP), which form the mucus matrices in marine snow.

The contribution of Dark particles (M3, M6, M8, M15, M16) to the MS community increases with depth from up to 40% in the epipelagic layer to up to 80% in the mesopelagic. They show a stronger seasonal variability in Benguela and Tasmania compared to Angola and Equator. They are weakly (rs<0.3) or not correlated to *in situ* Chla but they are all correlated to LLC with maxima after 10-15 days. All morphotypes are more correlated to *in situ* plankton counts (Trichodesmium, Rhizarians and small copepods for all but M15 which is only correlated to copepods) than *in situ* Chla suggesting that zooplankton may be an important source of material to produce these categories. Their mostly round shape suggests coagulation and fecal pellet production as possible mechanisms to aggregate the different source particles. The contribution of **fluffy** particles (M4, M5, M14) to the MS community decreases with depth in Equator and Angola from up to 50% in the epipelagic layer down to 10% in the mesopelagic. In Benguela or Tasmania they have lower but more variable contributions. M4 and M5 show less seasonality than M14 (Fig 5). All morphotypes are

more correlated to LCC and *in situ* plankton counts (Trichodesmium, Rhizarians and small copepods) than *in situ* Chla suggesting that long lasting phytoplankton production and zooplankton sloppy feeding or fragmentation may produce these categories. **Elongated** particles (M7, M9, M10, M12 and M17) are clearly restricted to the upper water (apart from M10 at the Equator) and have a seasonal cycle. The seasonal cycle is most pronounced for M17 and least pronounced for M7 (except in Tasmania). Their contribution to the MS surface community increases with latitude from 40 to 90% during the productive season. In the mesopelagic layer, their contribution decreases to 20-40% notably at high latitude. Apart from M7, they are more correlated (rs=) to the in situ Chla than any zooplankton counts (small copepods rs=) suggesting that M9, M10, M12 and M17 are phytodetritus while M7 (both correlated to Chla and plankton counts) may also contain elongated fecal pellets. Their LLC does not increase with the time lag suggesting that they are fresh phytoplankton material. Among the elongated group, M17 is the only morphotype correlated to in situ Chla but not to the Lagrangian Chla and negatively correlated to plankton (except big copepods). In addition, it is the sole morphotype with M10 to be negatively correlated with in situ temperature. Their elongated form and their length (X mm) suggest that they are colonies or cells rather than large particles produced by small phytoplankton cells. For these reasons, elongated particles may contain elongated fecal pellets (mostly in M7), fresh phyto-detritus (M9, M10, M12) and even living filaments of phytoplankton (M17) mostly in the high latitudes. Interestingly, M12 and M17 can contribute to more than 80% of the summer's productive surface water off Benguela and off Tasmania compared to less than 10% at the two other sites. The contribution of **agglomerates** (M11 and M13) varies between 5 and 10% of the MS in both layers. Their occurrence requires long lasting productive periods as suggested by their low correlation with in situ Chla and strong correlation with LCC after 15 days. Our results suggest that they are produced in the upper water column and exported to the deep with more efficiency for M13 than M11.

SM 7: In situ environmental and plankton vertical properties

The depths of the mixed layers (Fig. 2, (d)) determined by the MLD_bio are shallower and more stable in tropical regions, with averages of 45 ± 15 m in Angola and 67 ± 18 m in Ecuador. Conversely, in high-latitude regions, these averages are 111 ± 59 m in Benguela and 122 ± 98 m in Tasmania. These differences are mainly explained by the southern seasonality and intense stratification of tropical waters. During the southern winter, the bio MLD reaches average depths of 142 ± 58 m in Benguela and 254 ± 136 m in Tasmania, compared to shallower and less variable depths during the southern summer, with 56 ± 15 m in Benguela and 75 ± 30 m in Tasmania.

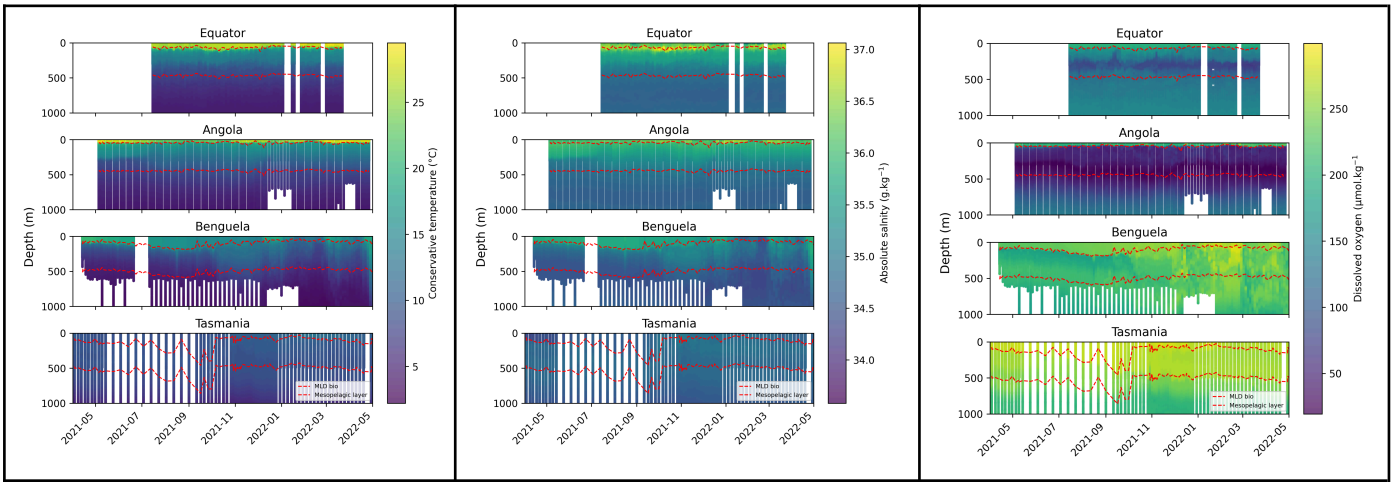

Supp. Fig. 7 Annual variability of environmental factors, A) Temperature, B) Salinity and C) Dissolved oxygen and depth horizon of the MLD and the two mesopelagic layers used to assess plankton and marine snow community composition.

The vertical distribution of chlorophyll varies according to latitude. In tropical regions, the profile is relatively stable, with a maximum chlorophyll concentration generally observed between 30 and 60 metres. In Ecuador, this maximum reached 6.5 mg m^{-3} in September 2021 at a depth of approximately 50 metres. In Angola, the dynamics are marked by peaks of abundance at the surface, with peaks reaching 11.9 mg m^{-3} at a depth of 10 metres in February 2022. Seasonality is clearly observed in high-latitude regions with peaks in chlorophyll a and particles (Bbp, MiP and MaP) abundance during the southern summer between November and March. Maximum values reach 5.4 mg m^{-3} in December 2022 in Tasmania and 1.3 mg m^{-3} in Benguela in January 2022, at a depth of approximately 10 metres.

MAPs and MIPs are mainly concentrated in the mixed layer in all regions. Angola is the region with the highest abundances, averaging 192 ± 175 part L^{-1} for MIPs and 5.5 ± 7.1 part L^{-1} for MAPs, while Ecuador has lower abundances, averaging 143 ± 75 part L^{-1} for MIPs and 2.7 ± 1.9 part L^{-1} for MAPs. In high-latitude regions, Tasmania was richer, with an average of 100 ± 122 part L^{-1} for MIPs and 1.3 ± 2.5 part L^{-1} for MAPs. Benguela has the lowest abundances, with an average of 65 ± 39 part L^{-1} for MIPs and 0.7 ± 0.83 part L^{-1} for MAPs. Tropical regions are richer in particles than regions at higher latitudes. However, extreme production events can lead to high abundances in high-latitude regions. Thus, for MAP abundances, the 99th percentile in Tasmania reaches 12.6 part L^{-1} and 4.7 part L^{-1} for Benguela, compared to 37.4 part L^{-1} for Angola and 9.9 part L^{-1} for Ecuador. For MIP, these values reach 567.9 part L^{-1} in Tasmania, 199.1 part in Benguela, 902.2 part L^{-1} in Angola and 380.3 part L^{-1} in Ecuador.

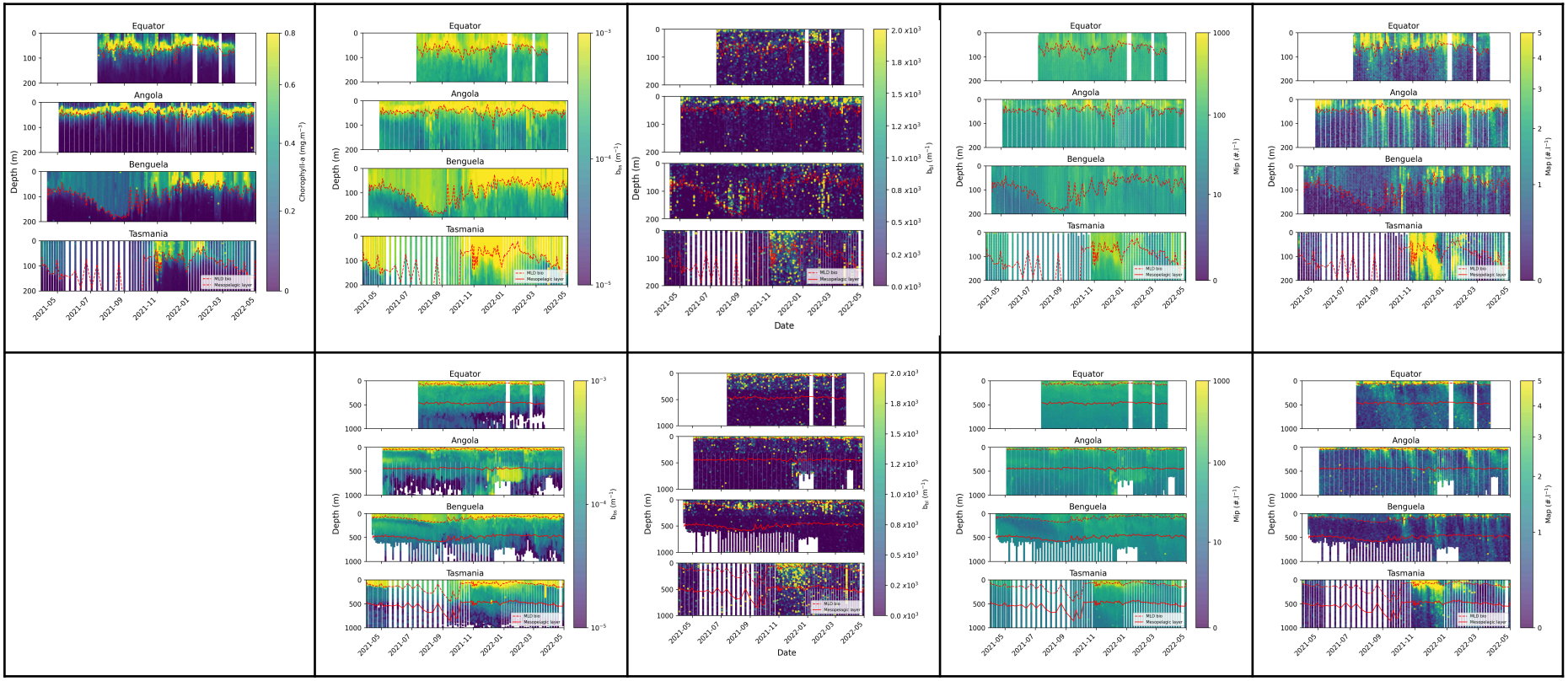

Supplementary Figure 8: Annual cycle of Chla, bbs, bbl, Mip and Map in the upper 200 m depth water column (first row) and in the upper 1000m depth (second raw). The depth layers limits used to integrate plankton and marine snow are indicated by the red lines.

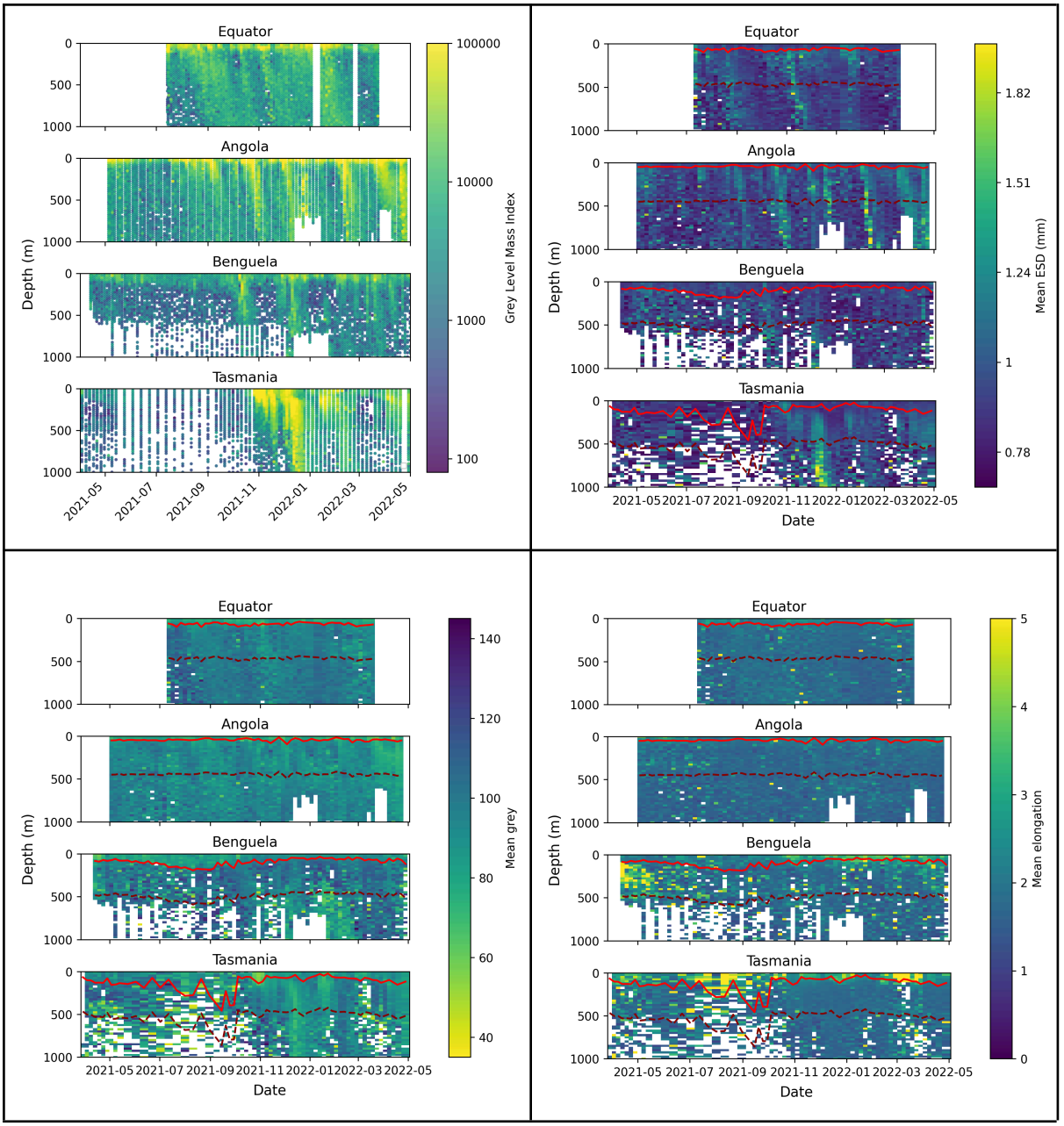

Supplementary Figure 9: Annual cycle of MaP properties, a) gray Level mass index (proxy of total particle mass), mean size (ESD), b) mean grey level (transparency) and c) mean elongation in the upper 1000 m depth water column. The depth layers limits used to integrate plankton and MS counts are indicated by the red lines.

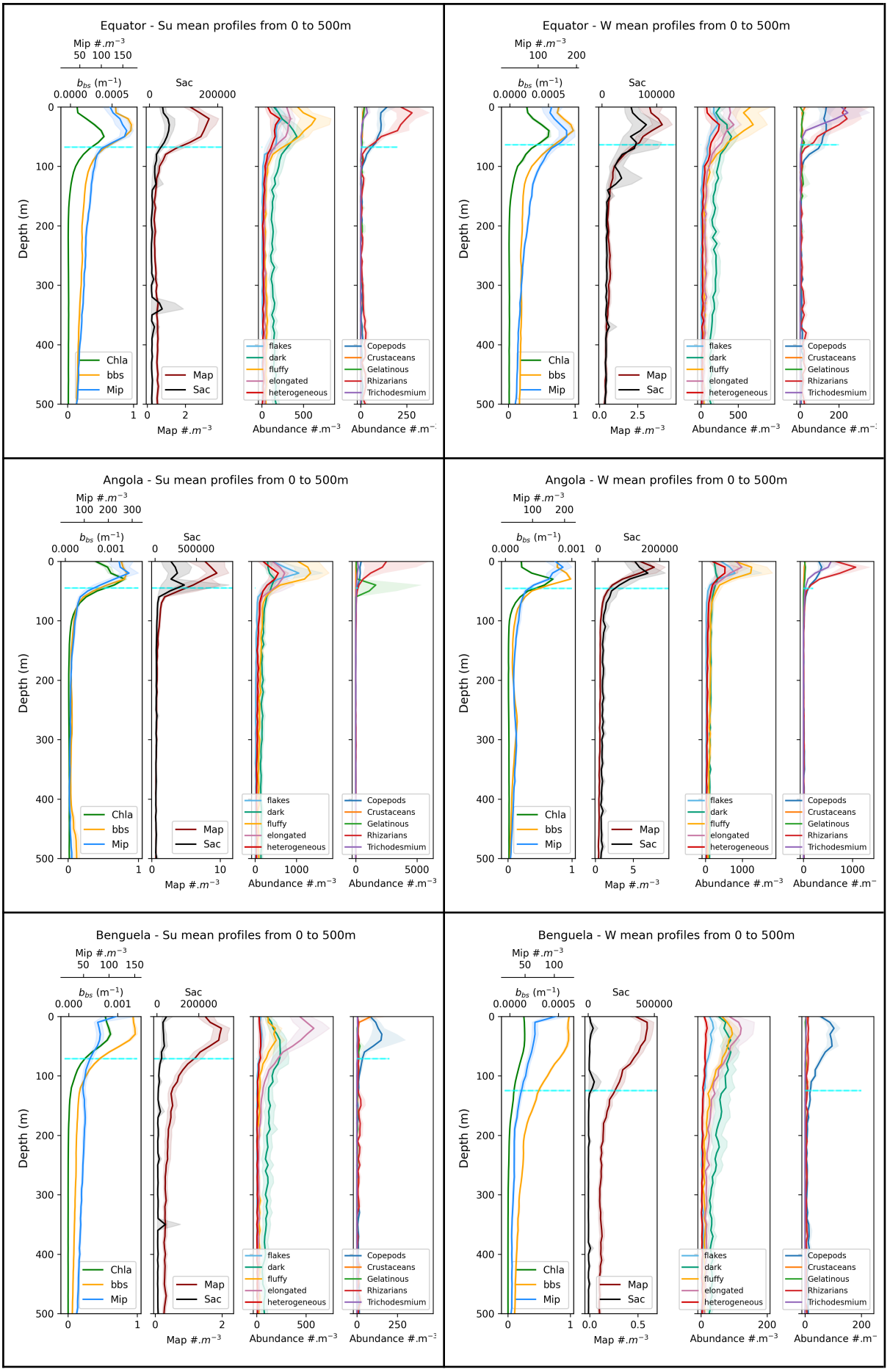
Equator - Su mean profiles from 0 to 500m
Equator - W mean profiles from 0 to 500m
Angola - Su mean profiles from 0 to 500m
Angola - W mean profiles from 0 to 500m
Benguela - Su mean profiles from 0 to 500m
Benguela - W mean profiles from 0 to 500m
Depth (m)
Mip #.m⁻³
bbs (m⁻¹)
Sac
Chla
bbs
Mip
Map
Sac
Map #.m⁻³
flakes
dark
fluffy
elongated
heterogeneous
Abundance #.m⁻³
Copepods
Crustaceans
Gelatinous
Rhizarians
Trichodesmium

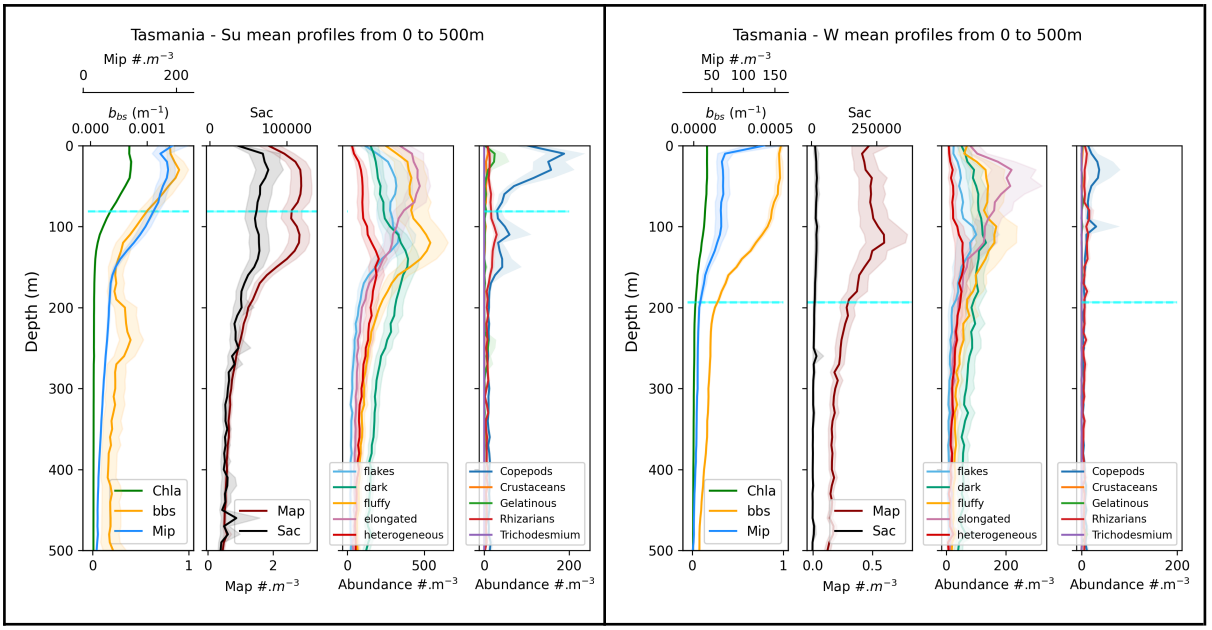

Supplementary Figure 10 : Mean vertical profiles of all particle types, Chla, bbs, MiP, MaP, SAC and major plankton taxa in summer (left panels) and winter (right panels) at the Equator (first row), Angola (second row), Benguela (third row) and in Tasmania (fourth row). The envelope is the confidence interval at 95% of the mean.

SM 8: Marine snow community composition dynamics

To study the structure of morphological particle communities and planktonic communities in each layer considered, we perform PCA on the concentrations of each taxonomic and morphological group transformed using the Hellinger transformation. The impact of the environment on the structure of detritus communities is studied by performing canonical redundancy analysis (RDA) (Rao 1964) and The impact of the environment on the structure of detrital communities is studied by performing canonical redundancy analysis (RDA) (Rao 1964) and partial canonical redundancy analysis (p-RDA), taking as the response variable matrix the matrix of morph abundances transformed using Hellinger and as explanatory variable matrices the matrix of environmental variables transformed using the Yeo-Johnson transformation and the matrix of planktonic taxon abundances transformed using Hellinger.

In the PCA, the two first axes together explained 56% of the total variation. Differences in relative particle composition among samples were primarily driven by the contributions of three morphotypes, dark (as positive PC1), elongated (as negative PC1 and positive PC2), and the assemblage of flake, fluffy and agglomerates (negative PC1 and negative PC2). PC1 discriminates very well the epipelagic communities from the lower mesopelagic ones at all sites and during all year round while the upper pelagic has an intermediate pattern (Fig. 3B). During summer in the Benguela time series, a small deviation in the lower pelagic toward lower PC1 values is observed indicating that the marine snow community composition more closely resembled that of the surface. PC2 shows a clear seasonal signal for Benguela and Tamasnia regions in the epipelagic (small circles with $PC1>0$ and large circles for $PC1<0$) and to a lesser extent in the upper- and lower- mesopelagic layer. The temporal patterns of the 17 children morphotypes correspond quite well to the parent classification at 5 morphotypes. This correlation is less observed for M7 among elongated and for M16 among dark.

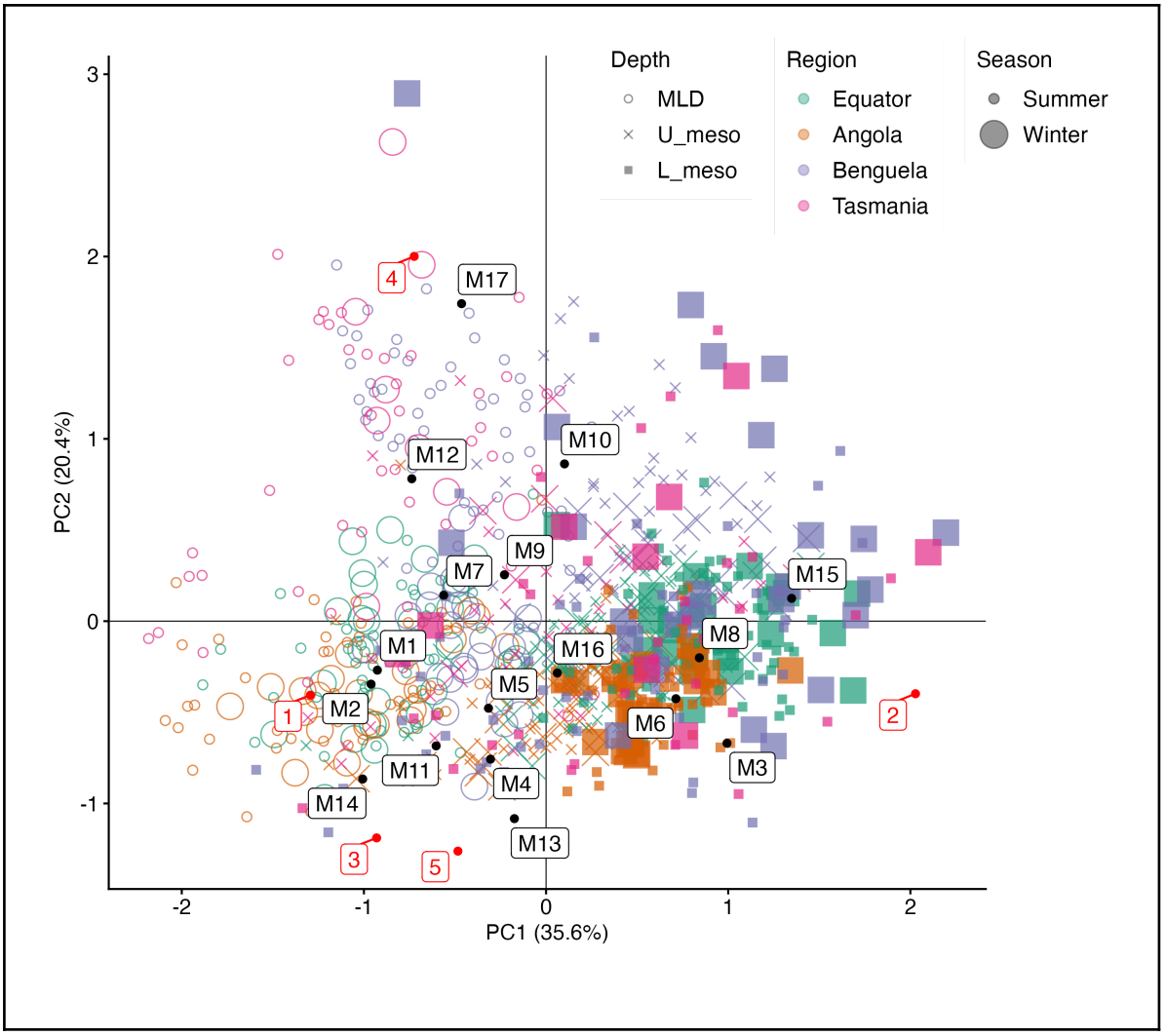

Supplementary Figure 11: A) PCA space of the 868 points (date*layers*regions) considering the time series in the three depths in all the regions (Angola, Benguela, Equator and Tasmania) as determined from their community compositions in the epipelagic (circle) and lower- (cross) and upper- (square) mesopelagic layers during summer and winter. The size of the symbols indicate the season.

RDA analyses are performed by layers separately to assess the importance of temporal environmental drivers for marine snow. The RDA combining planktonic communities and environmental variables is significant (p-value = 0.001) in both layers with an adjusted $R^2 = 0.44$ and $R^2 = 0.09$, respectively in the epipelagic and mesopelagic. For the epipelagic, the first two axes explain 48% of the constrained variance (Fig. 4). The first axis contrasts elongated communities with heterogeneous agglomerate communities and distinguishes high-latitude regions from low-latitude regions (F(1) = 247.8, p-value = 0.001). The second axis is a gradient of dark (positive values), opposed to Bbs, MIP and MAP (F(1) = 73.1, p-value = 0.001). The variance partitioning performed on the unselected models revealed higher explained variability by the environment alone (18%) compared to plankton alone (8%), with a shared contribution of 26%. Flakes, fluffy and agglomerates are dominant in Equator, Angola and Benguela (during austral winter only), which are warmer systems dominated by Collodaria, and other Rhizaria. In contrast, elongated aggregates dominate in Tasmania and Benguela (during austral spring and summer only), which are colder systems characterized by mesoscale activity and dominated by large copepods and Eumalacostraca. Dark aggregates are more associated with systems dominated by small copepods, thecosomata, ostracods and thaliacea. Time series of RDA1 and RDA2 indicate a stronger seasonal cycle in the community composition of marine snow in Benguela and Tasmania compared to Equator and Angola. Results for the mesopelagic layer show that the two axes explain 7.4% of the constrained variance (Supp Fig. 7).

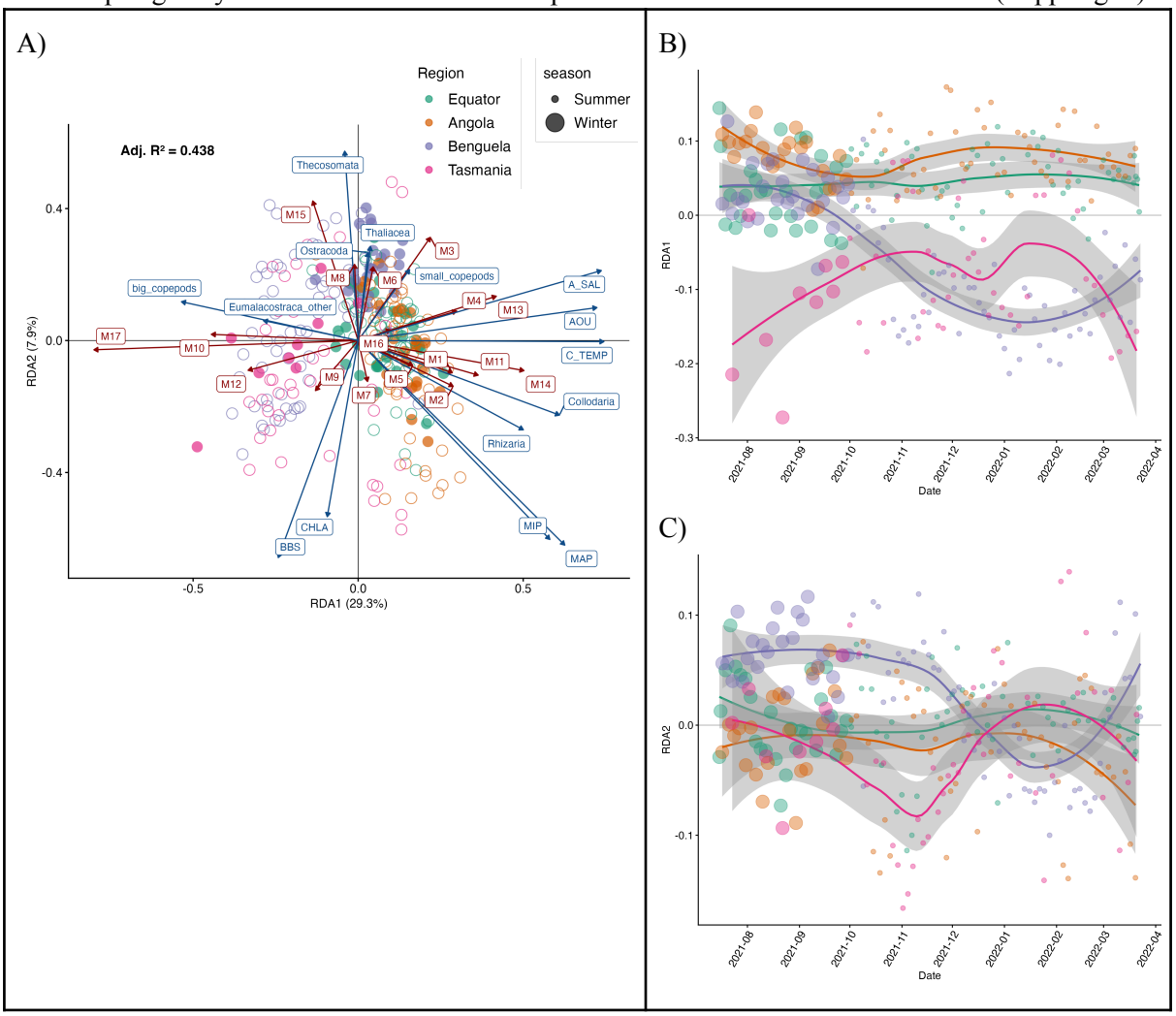

Supplementary Figure 13: A) RDA space of the 293 profiles as determined from their community compositions in the epipelagic layers. B) and C) respectively time series of coordinates on the first and second axis.

In the mesopelagic layers, the RDA combining planktonic communities and environmental variables is significant in but low (adjusted R^2 = 0.1, p-value = 0.001) and the first two axes explain 8.5% of the constrained variance (Supp. Fig. 14). The first axis opposes systems dominated by dark aggregates from systems where flakes prevail (F(1) = 15.8, p-value = 0.001) . The second axis is a gradient of proportions of light spheres and heterogeneous aggregates, along a gradient of MAP, AOU and salinity (F(1) = 9.6, p-value = 0.001). No plankton taxa appears to be important for the community composition of marine snow. The variance partitioning performed on the unselected models reveals that most of the explained variability (6%) is driven by the environment alone and a simultaneous variance share between plankton and environment of 3%. Seasonal variability is only observed in Tasmania and Benguela with higher contributions of flakes and fluffy morphs in summer.

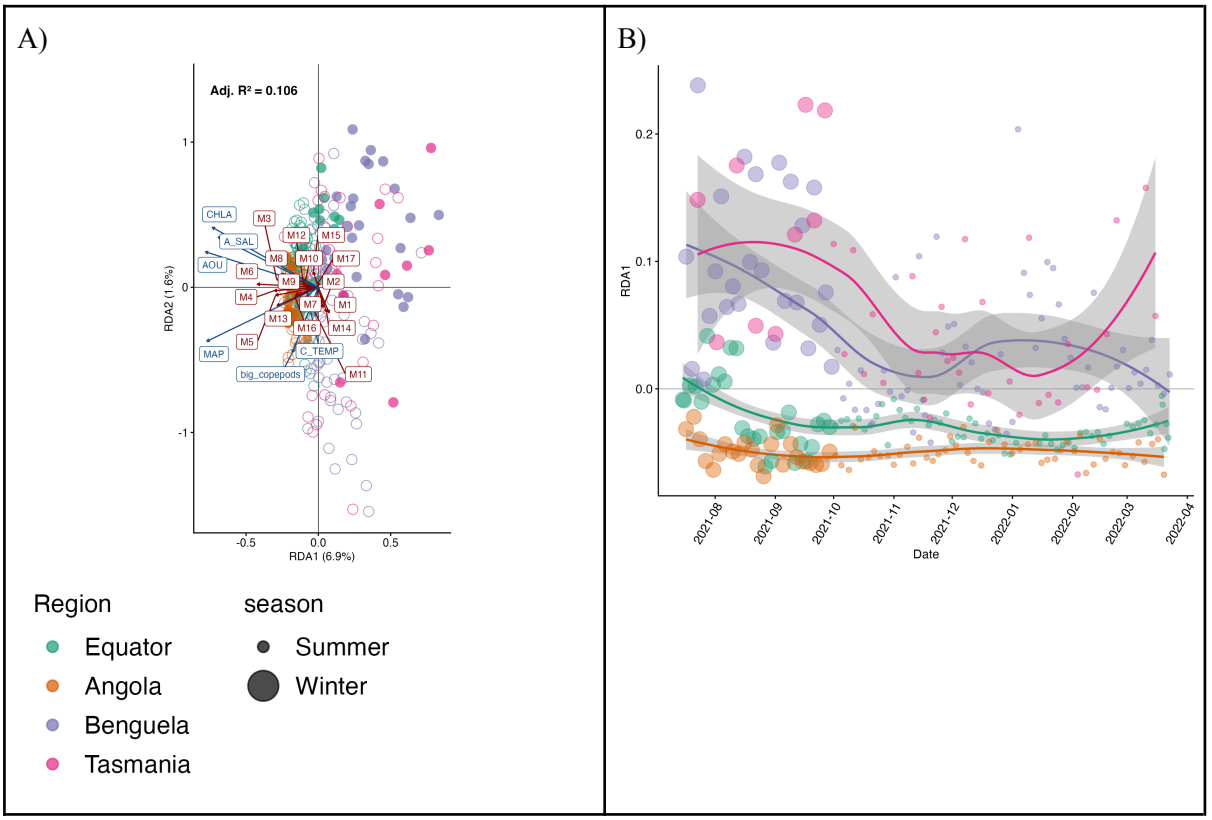

Supplementary Figure 14: A) RDA space of the 282 profiles as determined from their community compositions in the lower mesopelagic layers. B) time series of coordinates on the first axis.

SM 10: Transfer efficiency

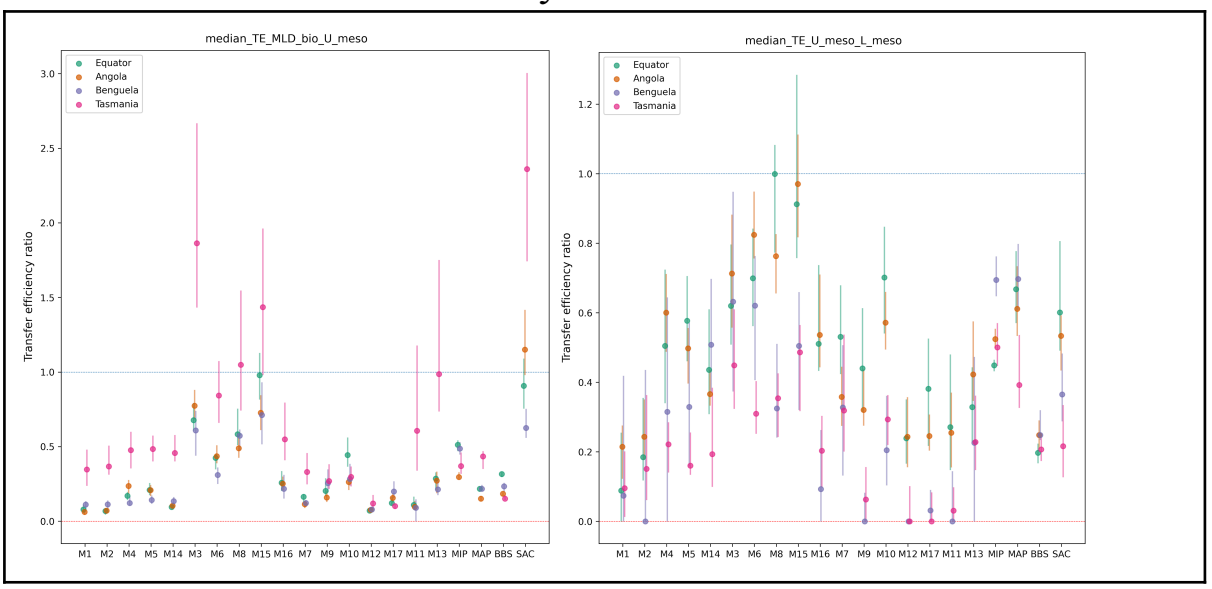

Supplementary Figure 15: Ratio between mixed layer and upper mesopelagic concentrations (left) ratio between upper mesopelagic and lower mesopelagic concentrations of 17 morphotypes.

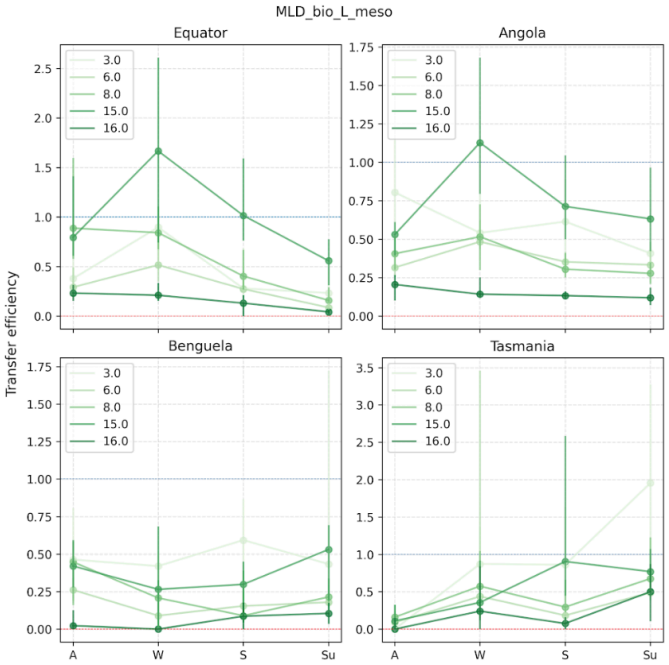

Supplementary Figure 16: Ratio between epipelagic and mesopelagic concentrations of the dark morphotypes.

Bibliography

1. Trudnowska, E. *et al.* Marine snow morphology illuminates the evolution of phytoplankton blooms and determines their subsequent vertical export. *Nature communications* **12**, 2816–2816 (2021).
2. Soviadan, Y. D. *et al.* Marine snow morphology drives sinking and attenuation in the ocean interior. *Biogeosciences* **22**, 3485–3501 (2025).
3. Accardo, A. *et al.* Massive and localized export of selected marine snow types at eddy edges in the South Atlantic Ocean. *EGUsphere* **2024**, 1–29 (2024).
4. Habib, J. *et al.* Marine snow surface production and bathypelagic export at the Equatorial Atlantic from an imaging float. *EGUsphere* **2024**, 1–27 (2024).
5. Accardo, A. *et al.* Intense and localized export of selected marine snow types at eddy edges in the South Atlantic Ocean. *Biogeosciences* **22**, 1183–1201 (2025).
6. Alldredge, A. L. & Silver, M. W. Characteristics, dynamics and significance of marine snow. *Prog. Oceanogr.* **20**, 41–82 (1988).
7. Laurenceau-Cornec, E. C., Trull, T. W., Davies, D. M., Christina, L. & Blain, S. Phytoplankton morphology controls on marine snow sinking velocity. *Marine Ecology Progress Series* **520**, 35–56 (2015).
8. Durkin, C. A. *et al.* A visual tour of carbon export by sinking particles. *Global Biogeochemical Cycles* **35**, e2021GB006985 (2021).
9. Song, Y., Omand, M., Durkin, C. A., Estapa, M. L. & Buesseler, K. O. GelCam: Visualizing sinking particle flux via a polyacrylamide gel‐based sediment trap. *Limnology and Oceanography: Methods* (2025).